Retrieving avalanche basal friction law from high rate positioning of avalanches

G. Pulfer, Mohamed Naaim, Emmanuel Thibert, A. Soruco

Pulfer G., Naaim M., Thibert E., Soruco A. Retrieving avalanche basal friction law from high rate positioning of avalanches. International Snow Science Workshop (ISSW 2013), Grenoble Chamonix-Mont-Blanc, France, October 7-11, 2013. pp. 1418-1424

Retrieving avalanche basal friction law from high rate positioning of avalanches

Pulfer G.[1] *, Naaim M.[1] , Thibert E.[1] , Soruco A. [2]
[1] Irstea, Grenoble, France
[2] IGEMA, La Paz, Bolivia

ABTRACT : The Voellmy avalanche basal friction parameters are retrieved from high rate positioning of artificially released avalanches. Two dense snow avalanches were triggered at the Lautaret full-scale test site on December 19th 2012 and February 13th 2013. Their fronts were tracked thanks to an accurate photogrammetric system. Couples of images were acquired at 1 frame per second with 2 APS-C DSLR synchronized cameras set at 800 meters from the avalanche track. 9 control points are used for image orientation and the typical precision for this measurement is around 0.2m for any point of the avalanche front. For the two avalanches, velocities are determined on several points of the front along different directions orthogonal to the flow. In order to retrieve rheological parameters of the avalanche, the front is considered as a hydraulic intumescence and the relation between its velocity and the avalanches properties is developed in the sliding block model framework. The Voellmy friction parameters in the accelerating, steady and decelerating phases are quantified and discussed.

KEYWORDS : friction parameters, Avalanches, Front dynamics, Photogrammetry, Voellmy, Rheology.

MOTS CLES : Paramètres de frottement, Avalanches, Dynamique du front, Photogrammétrie, Voellmy, Rhéologie.

1 INTRODUCTION

Avalanche hazards are important concerns for population in mountain areas. Risk characterization and avalanche hazard zoning in inhabited areas have recourse to avalanche flow simulation. The main approaches to model avalanches are based on the Saint-Venant equations. In these last, snow rheology is assimilated to a basal friction. Basal friction law remains difficult to quantify accurately because the physics of flowing snow is complex and highly variable. Here, we propose to determine the friction parameters expressed in the Voelmy formalism using a high rate positioning of the avalanches from the beginning of the flow to the run-out.

2 METHOD

Our objective is to identify Voellmy friction parameters of an avalanche using a high rate positioning in three dimensions during the avalanche flow. The studied avalanches are artificially released, this allows to characterize with a good precision the physical properties of snow and the initials conditions.

2.1 Lautaret test site

Our experiments are performed at the Lautaret full-scale avalanche test site. This test site is located in the French Alps in the Hautes-Alpes department (Fig. 1). This experimental test site holds a succession of avalanche path oriented on the South-East of the Chaillol Mountain. One path referred as path n°2 has been specially instrumented to study the dynamics of dense avalanche flow. This path is 450 m long between 2400 and 2100 m a.s.l. Its first part, where the acceleration flow occurs, is steep with a typical average inclination of 37° and a maximum value around 45° in the starting area. This part is steep-sided ; around 10 m-wide so the flow is almost well channelized during 200 m. The second part is mainly the run-out zone and the slope is flatter around 30°. At the transition between the two parts there is a road (Col du Galibier road, open in summer), and, just over this point, a steel pylon structure is set-up to measure

∗. *Corresponding author address:* Pulfer G., Irstea, UR ETGR, 2 rue de la Papeterie - BP 76, F-38402 Saint-Martin-d'Hères, France,
Tel: + 33 4 76 76 27 58; Fax: +33 4 76 51 38 03;
Email: gaetan.pulfer@irstea.fr

the thickness of the flow, its velocity and pressure along time. This pylon corresponds to the point M_{28} on Fig. 2.

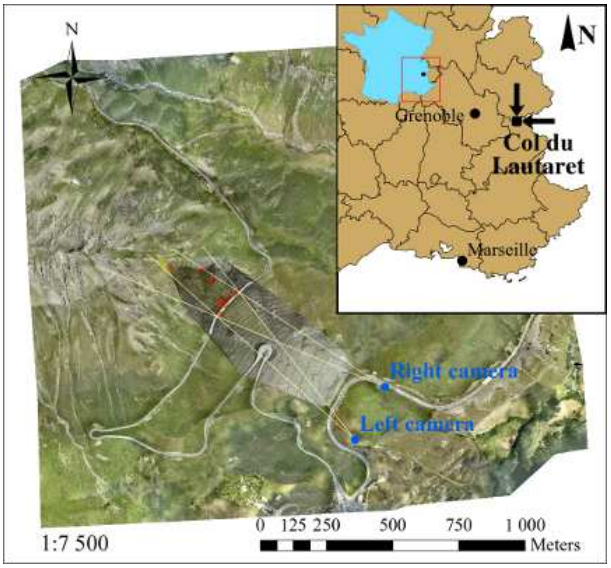

FIGURE 1 – Geographic position of the Lautaret path. Ortho-photography at $1 : 7500$ scale with the position of path number 2. Contour lines at 10 m interval. Blue dots are the position of the camera for the photogrammetric device, the yellow line represents the field of view of the lens (focal length : 85 mm) and the yellow polygon defines the area where photogrammetric measurements are possible. Red symbols (⊗) indicate the position of the GCP used for image orientation.

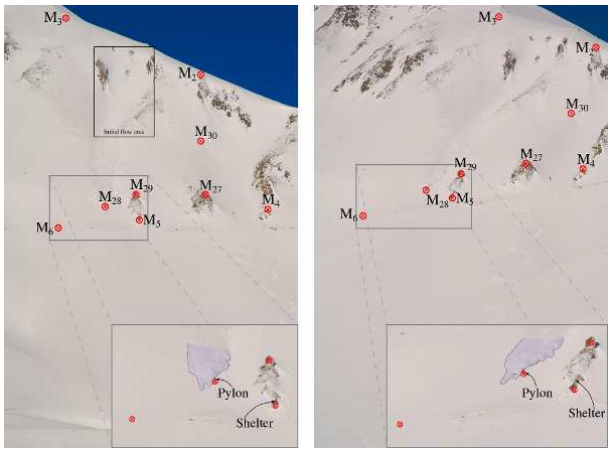

FIGURE 2 – Couple of image used for the photogrammetric measurement for the 13th February 2013 avalanche, the position of the GCP are shown on both images (⊗). The initial flow area is defined (position of multiple flow in Fig. 3). A zoom in the area of the pylon measurement shows the position of the front at time $t = 13s$ in left and right images.

2.2 *Avalanches conditions*

Two different events are considered in the present study : the first one is an avalanche released on December 19th 2012 and the second one is an avalanche released on February 13th 2013 (image of this avalanche on Fig.2 and 3). The behaviour of these two avalanches are mixed, i.e. composed of a dense part and, above it, an aerosol phase appearing when the velocity is high enough for setting snow particles in saltation. In order to characterize as finely as possible the properties of the snow involved in the flow, a density, temperature and hardness profile of the released layer was measured. Snow grain type and dimension was also characterized. On the 13th February, the avalanche was released at 11h58. At this time, air temperature was about $-10°C$. A 0.25 m thick layer of fragmented and decomposing particles was released in the avalanche path. Its mean density was 250 kg/m^3, ranging within 270-225 from bottom to the surface. In the released layer, particle sizes were less than 0.5 mm. Snow temperature was between $-4.7°C$ and $-5°C$. Hardness was fist (hand index) and measured as 20 N in Ram Resistance Equivalents. Unfortunately, we do not have such a detailed snow characterisation for the avalanche released on the 19th December 2012.

2.3 *Avalanche front dynamics*

Avalanches in path n°2 on the Col du Lautaret flow on an almost simple topography : there is no particular obstacle over the flow track. Nevertheless, we can see in Fig. 3 that some multiple and complex avalanches can appear in the departure area depending on how the first snow layers are destabilized by the release system. Indeed, in the initial flow area (define in Fig. 2) for the 13 February 2013 avalanche, four different flows occurring in the same time can be identified. These sub-avalanches, referred as F_1, F_2, $F_{2\alpha}$ and $F_{2\beta}$ (Fig. 3), exist at the same time. After few seconds, their flows merge to create a single avalanche that we can track until the run-out. It is nevertheless important to consider these specific flows at the beginning of the avalanche release, because their velocities are significantly different and such flows

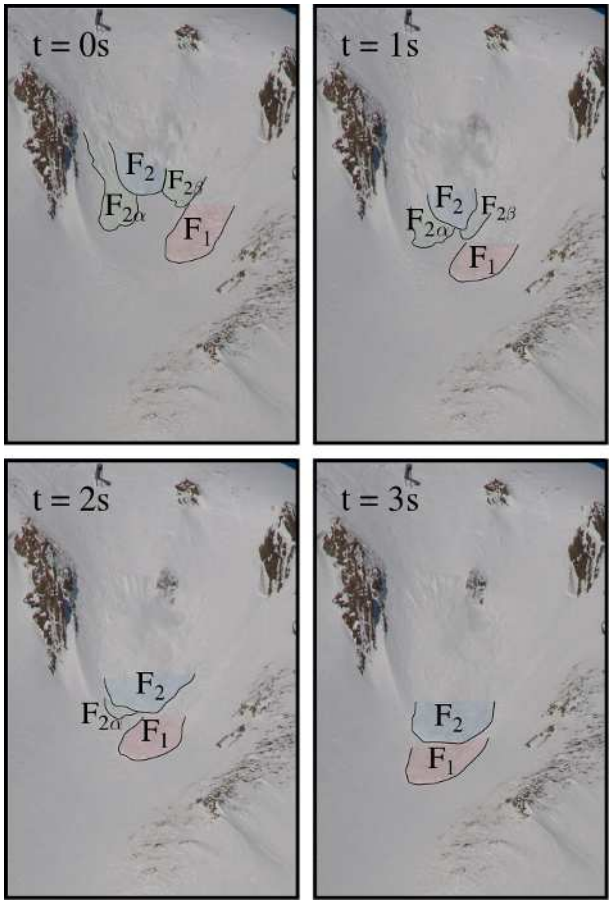

FIGURE 3 – Four different images of the 13th February 2013 avalanche separated in time by one second in the initial flow area defined in Fig. 2. The multiple complex flows named F_1, F_2, $F_{2\alpha}$ and $F_{2\beta}$ are drawn and show the interest of the photogrammetric method and the possibility of photo-interpretation.

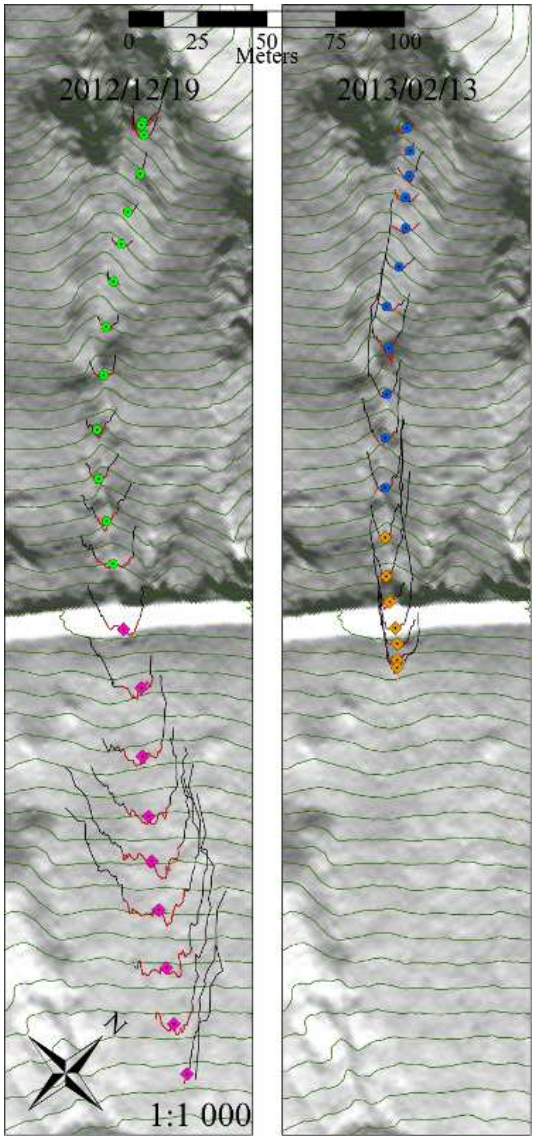

FIGURE 4 – Front position of the avalanche at each second for the event of 19th December 2012 from the right and the 13th February 2013 from the left. Green lines are the contour lines at 5 m interval. Black lines are avalanche front positions as obtained by the photogrammetric method at each second. Red lines are the selected points used for the determination of the centroid. The accelerated phase of the flow is represented by circles (green for the 2012/12/19 and blue for the 2013/02/13 event), while diamonds depict the decelerated one (purple for the 2012/12/19 and orange for the 2013/02/13 event).

spread with their own dynamics during a non negligible time frame. Avalanche F_1 and F_2 indeed flow simultaneously during 7 seconds.

The photogrammetric method that we have developed allows to follow the avalanche front at high frame rate. This is not possible with other topographic survey techniques as for example total stations or laser scanning measurements. With our device, couples of images can be captured at 1 frame per second during the total time of the avalanches. This equipment is particularly interesting as it also allows to carry out some photo-interpretation which are essential to discriminate between the different flows that may develop at the beginning of the release as mentioned above.

The device is composed of two non-metric numerical reflex cameras (DSLR) Nikon D2XS. The sensor produces an image of 12.21 mega pixels

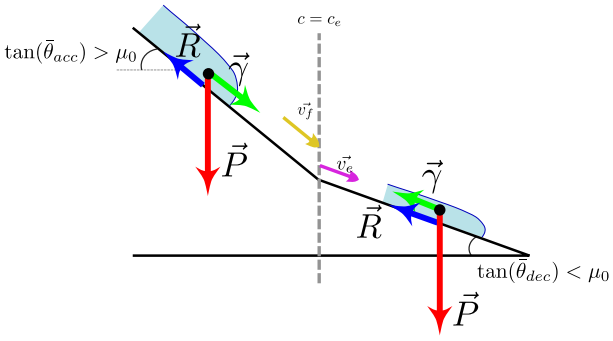

FIGURE 5 – Equilibrium of motion in the accelerating and decelerating part of the flow, situation of the sliding block model.

(4288×2848) with an APS-C size (23.7×15.7 mm) whose pixel size is 5.5198 μm. The lenses mounted on the cameras are fixed focal lenses 85mm f/1.4 AF-S series D from Nikon Corporation. As a non-metric device, these commercial cameras need a specific calibration to quantify the focal length, the decentration (non-radial distortion) and the radial distortion. Synchronisation between the two cameras is perform using the master clock of a Campbell CR3000 micro logger which provides a rate within a precision of $\sigma_{t_{clock}} = 5.7 \times 10^{-6}$s. Cameras are triggered thanks to wires connected to a control relay at a logger control port. Image orientations have been realised for each events using ORIMA software from Leica Geosystem. A network of nine ground control points (GCP red cross on Fig. 1 and 2) is visible on each image. The coordinate of these targets have been determined with a total station or a D-GPS. For a given avalanche and because cameras were rigidly set up, it was possible to obtain the same orientation for all the couple of images in the avalanche sequence.

After this image orientation step, each pixel is known in ground 3D coordinates and positioning can be achieved over the area intercepted by the couple of images. This defines the extent of the photogrammetric measurement as represented in yellow in Fig. 1. Restitution of each couple of image is made in stereoscopic vision under ArcGis software with help of the StereoAnalyst extension. The positions in time of each front are plotted with a temporal resolution of 1 second with the image sequence. (Fig. 4).

The theoretical photogrammetric error of positioning can be estimated following (Kraus and Waldhausl, 1998). Using 2 pixels as sighting error, ($2P_{size} \simeq 11\ \mu m$) the planimetric error is given by $\sigma_{xy} = 2P_{size}\frac{f}{B}$ and the altimetric error by $\sigma_z = 2P_{size}\frac{H^2}{fB}$ where $f = 85.51$ mm is the focal length obtained from calibration, $B = 230$ m is the photogrammetric base (the distance between the two camera (Fig. 1) and $H = 800$ m the mean distance to the measurement area. The theoretical error is therefore $\sigma^{Th}_{xyz} = \sqrt{\sigma^2_{xy} + \sigma^2_z} = 23$ cm. This sets the error for an individual point measurement. In practice, orientation residuals on the nine ground control points were found to be a little smaller. As obtained after the orientation step, those one are $\sigma_x = 11$ cm, $\sigma_y = 3.45$ cm and $\sigma_z = 1.83$ cm, so we obtain a total error $\sigma^M_{xyz} = \sqrt{\sigma^2_x + \sigma^2_y + \sigma^2_z} = 12$ cm. For the uncertainty analysis developed hereafter, we will consider the error calculated from the orientation residuals because it takes into account the individual sighting errors but averaged and distributed over all the GCP.

2.4 3D to 2D centroid-equivalent front

The result of photogrammetry positioning is a series of three dimensional data for the avalanche front position along time. In this preliminary study, we simply extract the friction parameters controlling the dynamics of avalanches (μ ; ξ) from the simple sliding block flow model in one dimension scheme (curvilinear abscissa). This is performed as a preliminary treatment before studying the friction coefficients with a Saint-Venant model making use of the 3D information of the data. A way to reduce our data set to a one dimensional problem is to consider the centroid of the avalanche front at each time $\bar{C_f}$ as obtain by :

$$\bar{C_f} = \left[\sum_{i=0}^{n} x_i \ ; \ \sum_{i=0}^{n} y_i \ ; \ \sum_{i=0}^{n} z_i\right]^T \qquad (1)$$

For the centroid calculation only a selection of points is considered among all restituted points. Lateral points of the front are excluded as they are not active in the dynamics of the front displacement. Selected points are defined from a line perpendicular to the flow direction joining the lateral edges of the front. Selection is performed manually. Results are displayed as red lines in Fig. 4. In the following, two phases of the flow will be considered to apply equations governing the velocity time evolution : an accelerating phase where the centroids are plotted with circles on Fig. 4 and a decelerating phases plotted with diamond on Fig. 4.

2.5 Velocity and friction law parameters

The avalanche front is considered as a hydraulic intumescence so that its velocity can be considered as same as the one of the center of mass of the avalanche assimilated as a sliding block model. The equilibrium of motion written of a finite volume V is given by :

$$\rho V \frac{d\vec{v}}{dt} = \vec{P} + \vec{R} \tag{2}$$

where ρ is the density of snow, P is the weight of the considered volume and R the basal resistance forces. After projection on the curvilinear abscissa c along the ground slope, the equation can be developed as :

$$\rho V \frac{dv(c)}{dt} = \rho V g \sin(\theta) - \rho V g \mu(v(c)) \tag{3}$$

where θ is the slope of the path, g the acceleration of gravity and $\mu(v)$ the Voellmy's friction coefficient defined by :

$$\mu(v) = \mu_0 + \frac{g}{\xi}(F_r^2) \text{ with } F_r = \frac{v}{\sqrt{gh}} \tag{4}$$

where μ_0 is the Coulomb's friction parameter, ξ the friction parameter due to the interaction between the snow and the air, F_r the Froude number and h the thickness of the flow. The density of snow is considered as a constant during the flow ($\rho = C^{te}$) and the acceleration term can be transformed into : $\frac{dv}{dt} = \frac{dv}{dc}\frac{dc}{dt} = \frac{1}{2}\frac{dv^2}{dc}$. As a consequence, the Eq. 3 can be written :

$$\frac{dv^2}{dc} = -\frac{2g}{\xi h}\cos(\theta)\left[\xi h(\tan(\theta) - \mu_0) - v(c)^2\right] \tag{5}$$

Two different phases have to be considered before integration : the accelerated part of the flow (see Fig. 5) between $c = 0$ and $c = c_f$ where $\tan(\bar{\theta}_{acc} > \mu_0)$ and the decelerated part (see Fig. 5) between $c = c_e$ and $c = c_f$ where $\tan(\bar{\theta}_{dec} < \mu_0)$.

2.5.1 Accelerated part of flow

When the accelerated phase is considered, the average slope ($\tan(\bar{\theta}_{acc})$) is higher than the friction coefficient μ_0. Equation 5 can be integrated between $c = 0$ and $c = c_f$ where the velocity is null in the starting zone ($v(c = 0) = 0$) and tends to a maximum velocity value $v(c_f) = v_f$ defined by :

$$v_f = \sqrt{\xi h(\tan(\bar{\theta}_{acc}) - \mu_0)} \tag{6}$$

After integration between $c = 0$ and $c = c_f$ we obtain the following expression for the velocity in the accelerated part of flow :

$$v = v_f\sqrt{1 - \exp\left(-\frac{2g}{\xi h}\cos(\bar{\theta}_{acc})c\right)} \tag{7}$$

2.5.2 Decelerated part of flow

On the contrary, in the decelerated phase the average slope ($\tan(\bar{\theta}_{dec})$) is lower than the friction coefficient μ_0. Equation 5 can then be integrated between $c = c_e$ and $c = c_1$ where $v(c_e) = v_e$ is the velocity at the entrance of the decelerating area and $v(c_1) = v_1$ is a limit velocity defined by :

$$v_1 = \sqrt{\xi h(\tan(\bar{\theta}_{dec}) - \mu_0)} \tag{8}$$

After integration between $c = c_e$ and $c = c_1$, the velocity in the accelerated area is given by :

$$v = \sqrt{v_1^2 + (v_1^2 + v_e^2)\exp\left(-\frac{2g}{\xi h}\cos(\bar{\theta}_{dec})c\right)} \tag{9}$$

3 RESULTS

3.1 Velocity and slope determination

The velocity v_m is calculated from the time evolution of the centroid position by :

$$v_m(t) = \frac{\bar{C}_f(t) - \bar{C}_f(t-1)}{\Delta t}, \tag{10}$$

where $\bar{C}_f(t)$ and $\bar{C}_f(t-1)$ are the centroids defined by Eq. 1 at time t and $t-1$ and Δt is the time interval between two couples of images (i.e here Δt=1s for the both avalanche). The uncertainty on the velocity is obtained considering 2 sources : the error in positioning σ_c due to photogrammetry and the time error due to frame triggering σ_t in relation to the master clock inaccuracy. This is written :

$$\sigma_v = \frac{\sigma_c}{\Delta t} + \frac{\Delta C \dot{\sigma}_t}{(\Delta t)^2}, \tag{11}$$

where σ_c is defined as $\sigma_c = 2\sqrt{2}\sigma_{xyz}^M$ working at the 95% confidence interval. As a consequence, the uncertainty on the curvilinear abscissa is equal to $\sigma_c = \pm$34 cm. The second term of equation 11 is in practice negligible because the maximum value of differences in successive ΔC each second, is typically 15-20 m and $\sigma_t = \sigma_{t_{clock}} = 5.7 \times 10^{-6}$s. As a

consequence $\frac{\sigma_c}{\Delta t} \gg \frac{\Delta C \cdot \sigma_t}{(\Delta t)^2}$ and we can reduce the expression of σ_v as :

$$\sigma_v = \frac{\sigma_c}{\Delta t} = \pm 34 \mathrm{cm/s}. \quad (12)$$

The velocity of each avalanche as a function of the curvilinear abscissa is plotted on Fig. 6a) and 6b) with error bars defined as one σ. The evolution of the slope along the curvilinear abscissa is defined by $s(c) = \tan(\theta(c))$ and retrieved from the measurements of the centroid positions using :

$$s(t) = \frac{\Delta \bar{z}}{\sqrt{\Delta \bar{x}^2 + \Delta \bar{y}^2}}, \quad (13)$$

where $\Delta \bar{x}$, $\Delta \bar{y}$ and $\Delta \bar{z}$ are the difference of each coordinate at time t and $t-1$. The uncertainty on the slope calculation is given by :

$$\sigma_s = \frac{1}{\sqrt{\Delta \bar{x}^2 + \Delta \bar{y}^2}} \left[\sigma_z + \frac{\sigma_x \Delta \bar{x} + \sigma_y \Delta \bar{y}}{\Delta \bar{x}^2 + \Delta \bar{y}^2} \right], \quad (14)$$

where σ_x, σ_y and σ_z are the orientation residuals defined in section 2.3. The evolution of the slope across the curvilinear abscissa is plotted on Fig. 6c) for both avalanches.

3.2 Extracting the friction law parameters

3.2.1 Accelerated part of flow

The velocity in the accelerated part, as obtained in Sec. 2.5.1, can be re-written considering two fitting parameters :

$$v = \alpha \sqrt{1 - \exp(-\beta c)}, \quad (15)$$

where $\alpha = v_f$ and $\beta = \frac{2g}{\xi h} \cos(\bar{\theta}_{acc})$. As a consequence we obtain this relation for the friction parameter ξh :

$$(\xi h)_{acc} = \frac{2g \cos(\bar{\theta}_{acc})}{\beta}, \quad (16)$$

We consider firstly the product ξh because it is necessary to make an hypothesis on h in order to estimate parameter ξ. The expression for μ_0 is :

$$\mu_{0acc} = \tan(\bar{\theta}_{acc}) - \frac{\alpha^2 \beta}{2g \cos(\bar{\theta}_{acc})} \quad (17)$$

The results for the friction parameter are given in Table 1. The goodness of fit is reasonable (Fig. 6) as we obtain for the 19th December 2012 a correlation of R^2= 0.8114 and a RMSE=3.337. Regarding the 13th February 2013 avalanche, the correlation is R^2= 0.9141 and a RMSE=1.375.

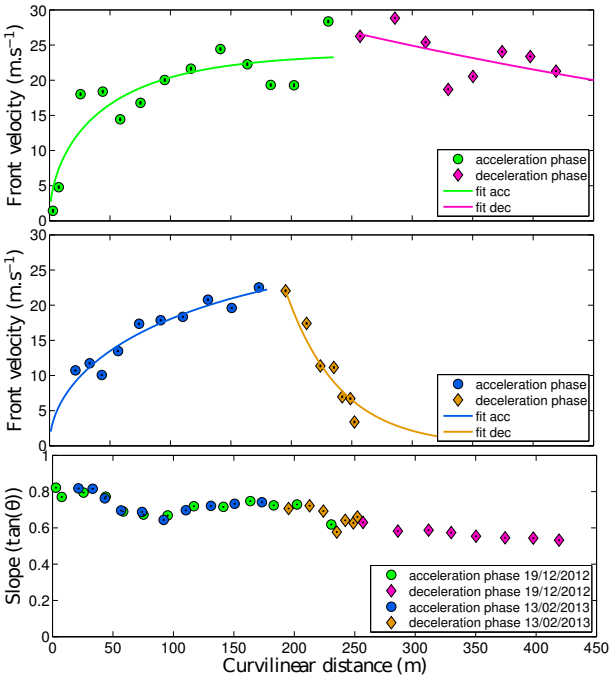

FIGURE 6 – Velocity as a function of the curvilinear abscissa for both avalanches. The accelerated part of the flow is plotted with dots, the decelerated one with diamonds and the fit curves with lines. The top graph represents the 19th December 2012 avalanche. Middle graph is the 13 February 2013 avalanche. Bottom graph is the slope evolution for each avalanche.

3.2.2 Decelerated part of flow

The velocity in the decelerated part can be as well formulated with two fitting parameters :

$$v = \sqrt{\gamma + (\gamma + v_e^2) \exp(-\delta(c - c_e))}, \quad (18)$$

where $\gamma = v_1^2$ and $\delta = \frac{2g}{\xi h} \cos(\bar{\theta}_{dec})$ and v_e the first velocity mesured at the abscissa c_e. As a consequence we obtain this relation for the friction parameter ξh :

$$\xi h = \frac{2g \cos(\bar{\theta}_{dec})}{\delta}, \quad (19)$$

The expression for μ_0 is :

$$\mu_{0dec} = \tan(\bar{\theta}_{dec}) - \frac{\gamma \delta}{2g \cos(\bar{\theta}_{dec})} \quad (20)$$

The results for the friction parameter are given in Table 2. The precision on the fitting parameter is correct (Fig. 6) as we obtain for the 19th December

Date	$\tan(\bar{\theta}_{acc})$	α	β	$(\xi h)_{acc}$	μ_{0acc}
2012 Dec 19	0.7267	23.8	1.324×10^{-2}	1200	0.25
2013 Feb 13	0.753	29.37	4.726×10^{-3}	3300	0.49

TABLE 1 – Friction parameters extracted from the accelerated part of the flow

Date	$\tan(\bar{\theta}_{dec})$	γ	δ	v_e	c_e	$(\xi h)_{dec}$	μ_{0dec}
2012 Dec 19	0.565	7.95	2.97×10^{-3}	26.25	256.85	5700	0.56
2013 Feb 13	0.646	3.65×10^{-7}	4.44×10^{-2}	22.05	192.27	400	0.64

TABLE 2 – Friction parameters extracted from the decelerated part of the flow

2012 a correlation R^2= 0.3219 and a RMSE=2.943. For the 13th February 2013 avalanche, R^2= 0.9250 and a RMSE=1.947.

4 DISCUSSION & CONCLUSION

The friction coefficient ξ give principally some information about the shape of the flow path of the avalanche. As all the avalanches considered in this study occurred in the same path, the value of ξ is expected to be approximately the same. Our results are significantly different event if we do not consider the height of the flow h. Nevertheless the value obtained in the accelerated part area are quite common and it is a good point as ξ predominate in this part of the flow.

The value of μ_0 are consistent with the field observation. For the 13th February 2013 avalanche, the high value obtained for μ_0 is coherent with the fact that the erosion was important in the path. We do not have measurement of snow properties for the avalanche released on the 19th December, but we suspect snow temperature to be lower as well as density. This may explain that the friction parameter is lower.

For the February avalanche, the value of μ_0 of 0.49 in the accelerated part is consistent with data from (Casassa et al, 1991) which gives 0.42 when adjusted for our snow temperature conditions ($-5°C$). Our result is nevertheless higher than the value reported by (Naaim et al., 2013) which indicates rather 0.275.

For both avalanches in the decelerated part, the values of μ_0 are very close to the values of $\tan(\bar{\theta}_{dec})$. The results of the decelerate part are more difficult to interpret. The first avalanche stopped outside of the area of the photogrammetric measurement and as a consequence we are not measuring overall the run-out phenomena and the final decrease in velocity has not been measured. Data is therefore not enough constrained, and, considering error bars, velocity can be considered as stationary which is consistent with the result μ_0 = $\tan(\bar{\theta}_{dec})$. This problem of image field of view will be solved with new lenses on cameras able to capture a larger area. Regarding the avalanche of February, it stopped quasi-instantaneously at 250 m from the released point. This is in relation with the presence of the road across the avalanche path at 220 m from the released point, which creates an important change in the topography. We suspect the flat part of the road to originate this important deceleration.

5 REFERENCES

Casassa, G., Narita, H., Maeno, N., 1991. Shear cell experiments of snow and ice friction. J. Appl. Phys. 69(6), 3745 3756. doi :10.1063 / 1.348469.

Kraus, K., Waldhausl, P. (Eds.), 1998. Manuel de photogrammétrie, principes et procédés.

Naaim, M., Durand, Y., Eckert, N., Chambon, G., 2013. Dense avalanche friction coefficients : influence of physical properties of snow. Journal of Glaciology 59, 216. doi :10.3189 / 2013JoG12J205.

6 ACKNOWLEDGEMENTS

The authors wish to thank Xavier Ravanat, Hervé Bellot, Fréderic Ousset and all those who contributed to measurements during avalanche release operations. Special thanks are due to M. Dumont, C. Carmagnola for snow characterisation performed on the 13th February 2013.